International Journal of Modern Engineering Research (IJMER)
www.ijmer.com Vol.2, Issue.4, July-Aug 2012 pp-2880-2884 ISSN: 2249-6645

Development of the A Three-Dimensional Magnetic-Field-Independent Absorbing Boundary Condition (Mfiabc) For Cold Magnetoplasma

Mohammad pourbagher[1], Javad nourinia[1] and Nader pourmahmud[2]
1(*Department of Electrical Engineering, Urmia university, IRAN*)
2(*Department of Mechanical Engineering, Urmia university, IRAN*)

Abstract: *A Three-Dimensional Cartesian-coordinate magnetized cold plasma algorithm has the capability to simulate wave behaviors in cold plasma under applied magnetic fields of arbitrary direction and magnitude. Plasma effects contributed by electrons, positive, and negative ions may all be included by this algorithm. A magnetic-field-independent absorbing boundary condition (ABC) is then proposed to truncate the computational domains that employ the cold plasma algorithm. To terminate the computational domain of the magnetized cold plasma FDTD algorithm an appropriate absorbing boundary condition (ABC) is required in order to model local regions of the Earth, or to model unbounded problems in the radial (vertical direction) on a global scale.*

Keywords: *Cold plasma, FDTD method, Boundary condition, PML, Ionosphere*

I. Introduction

In FDTD modeling, it is not possible to handle an open region problem directly since the data storage in a computer is limited by the size of memory. To mitigate this problem, an accurate and computationally efficient absorbing boundary condition (ABC) is needed to truncate the computational domain to suppress spurious reflections of the outgoing waves to an acceptable level. Its original split-field formulation introduced by Berenger [1] and various later reformulations, such as the uniaxial PML (UPML) [2], the convolutional PML (CPML) [3], and the NPML [4] provide orders-of-magnitude lower reflections and other advantages over previous versions of ABCs. However, the application of the standard PMLs has been limited to situations wherein the group and phase velocities of the incident wave are aligned in the same direction. When this is not the case, the PMLs cease to attenuate the field and can in fact act as an amplifier [5-7], which causes the algorithm to become analytically unstable. Becache et al. [6] confirms this instability with a theoretical analysis of PMLs for anisotropic media, for acoustic waves in elastic materials, and for EM waves. Cummer [7] has discussed the PML amplification phenomenon for the negative index materials (NIMs) in which the NIM materials exhibit both positive and negative refractive indexes over a range of frequencies. More recently, Chevalier et al. [8] encountered the same instability problem when modeling the antenna performance in a magnetized plasma for whistler waves. As pointed out in [7], this instability problem is inherent in the PMLs and is not implementation-specific. This poses a problem for modeling wave propagation in anisotropic media, such as whistler waves in magnetized cold plasma.

To address this issue, Cummer [7] has derived a modified PML solution for the negative index material (NIM) referred to as the NIMPML which is an adaptation of the previous NPML [4]. However, this method requires the simulated material to have a homogeneous permittivity and permeability (ε_r=μ_r), which is hardly the case for the ionospheric plasma medium that varies with both altitude and spatial position around the Earth. More recently, Chevalier et al. [5] presented in 2006 a new PML formulation referred to as the KPML which explicitly utilizes information on the *k*-vector direction of incident waves. Numerical tests in [5] demonstrate that KPML does not perform as well as the traditional CPML in open free-space problems, but it is stable and attenuates outgoing waves well for a case of whistler wave propagation in magnetized plasma media. However, the KPML can only be used as an effective ABC for dense magnetized plasma when the electron cyclotron frequency is much smaller than the plasma frequency. This is not the case for the lower region of the ionosphere. Moreover, the KPML algorithm is based on a single orientation of the background magnetic-field relative to each side of the FDTD grid and as such is not suitable for simulations involving spatially-varying magnetic-field directions such as for global modeling of the Earth-ionosphere system.

Considering these issues relating to the application of PMLs to magnetized plasma, we next consider Mur's ABC [9] as an alternative. Unfortunately, it is known that the original Mur's ABC exhibit an early-time instability for certain modeling scenarios. J. N. Hwang and F. C. Chen [10] have reported that the Mur's first-order ABC will cause instability problem for ADI-FDTD method. Zhang Yusheng and Wang Wenbing [11] have also confirmed that the second-order Mur's ABC combined with FDTD method to solve 3-D scattering problems is unstable. We encountered the same instability problem when applying the second-order Mur's ABC to the magnetized cold plasma algorithm. To solve this issue, Zhang and Wang [10] presented a new discretization scheme of the Engquist and Majda's second-order ABC equations [12] different from the scheme of Mur's ABC [9], which they claim is stable. However, we find through longer numerical tests that the early-time instability of Mur's ABC is simply replaced by a late-time instability in Zhang and Wang's scheme. In this article, the feasibility of a variation of Zhang and Wang's scheme is investigated to serve as an effective ABC for the 3-D FDTD magnetized cold plasma formulation. We choose this scheme despite its inherent late-time instability because it has the potential to provide an acceptable level of error regardless of the direction of the background magnetic-field, a capability

not provided by KPML. We then present a simple but very effective way to further delay the late-time instability of this magnetized plasma ABC.

II. Formulations

In 1977, Engquist and Majda [12] derived a theory of one-way wave equations suitable for analytical ABCs in FDTD simulations. The second-order approximations of these formulations at outer boundaries of a 3-D Cartesian space lattice can be expressed as follows.

$$\text{x=1} \rightarrow \frac{\partial^2 U}{\partial x \partial t} - \frac{1}{v}\frac{\partial^2 U}{\partial t^2} + \frac{v}{2}\frac{\partial^2 U}{\partial y^2} + \frac{v}{2}\frac{\partial^2 U}{\partial z^2} = 0 \quad (1)$$

$$\text{x=h} \rightarrow \frac{\partial^2 U}{\partial x \partial t} + \frac{1}{v}\frac{\partial^2 U}{\partial t^2} - \frac{v}{2}\frac{\partial^2 U}{\partial y^2} - \frac{v}{2}\frac{\partial^2 U}{\partial z^2} = 0 \quad (2)$$

$$\text{y=1} \rightarrow \frac{\partial^2 U}{\partial y \partial t} - \frac{1}{v}\frac{\partial^2 U}{\partial t^2} + \frac{v}{2}\frac{\partial^2 U}{\partial x^2} + \frac{v}{2}\frac{\partial^2 U}{\partial z^2} = 0 \quad (3)$$

$$\text{y=m} \rightarrow \frac{\partial^2 U}{\partial y \partial t} + \frac{1}{v}\frac{\partial^2 U}{\partial t^2} - \frac{v}{2}\frac{\partial^2 U}{\partial x^2} - \frac{v}{2}\frac{\partial^2 U}{\partial z^2} = 0 \quad (4)$$

$$\text{z=1} \rightarrow \frac{\partial^2 U}{\partial z \partial t} - \frac{1}{v}\frac{\partial^2 U}{\partial t^2} + \frac{v}{2}\frac{\partial^2 U}{\partial x^2} + \frac{v}{2}\frac{\partial^2 U}{\partial z^2} = 0 \quad (5)$$

$$\text{z=p} \rightarrow \frac{\partial^2 U}{\partial z \partial t} + \frac{1}{v}\frac{\partial^2 U}{\partial t^2} - \frac{v}{2}\frac{\partial^2 U}{\partial x^2} - \frac{v}{2}\frac{\partial^2 U}{\partial z^2} = 0 \quad (6)$$

where *U* denotes the scalar field components located at outer boundaries and *v* is the wave phase velocity, which is initially set to *c*, the velocity in free space. By central-differentiating the partial and second-order time and spatial derivatives of Equations (1)-(6) at time step *n* and at spatial locations half grid cell inside each boundary, one can obtain the well-known second-order Mur's ABC. In this article, by utilizing a different discretization scheme of Equations (1) - (6) than that utilized in Zhang and Wang's scheme [11], we derive our ABC expressions detailed as below. Our different approach from the so-called upwind-difference scheme of Zhang and Wang's ABC results in the same final form of the formulations as in Zhang and Wang's ABC. Here, we take Equation (1) as an example a derivation of the ABC expression for the $x = 1$ boundary. First, *U* around time step *n* and spatial location $(i+1, j, k)$ can be Taylor-expanded as

$$U^n_{i+1,j,k} = U^n_{i,j,k} + \left(\frac{\partial U}{\partial x}\Big|^n_{i,j,k}\right).\Delta x + \mathrm{O}(\Delta x^2) \quad (7)$$

From Equation (7), the first-order finite-difference approximation of the space derivative can then be obtained as

$$\frac{\partial U}{\partial x}\Big|^n_{i,j,k} = \frac{U|^n_{i+1,j,k} - U|^n_{i,j,k}}{\Delta x} \quad (8)$$

Applying Approximation (8) to both the spatial and time derivatives for the first term of Equation (1), we obtain the following:

$$\frac{\partial^2 U}{\partial x \partial t}\Big|^n_{1,j,k} = \frac{1}{\Delta t}\left(\frac{\partial U}{\partial x}\Big|^n_{1,j,k} - \frac{\partial U}{\partial x}\Big|^{n-1}_{1,j,k}\right) = \frac{1}{\Delta t}\left(\frac{U|^n_{2,j,k} - U|^n_{1,j,k}}{\Delta x} - \frac{U|^{n-1}_{2,j,k} - U|^{n-1}_{1,j,k}}{\Delta x}\right) = \frac{1}{\Delta t \Delta x}\left(U|^{n-1}_{1,j,k} - U|^{n-1}_{2,j,k}\right) - \frac{1}{\Delta t \Delta x}\left(U|^n_{1,j,k} - U|^n_{2,j,k}\right) \quad (9)$$

Next, the central-difference scheme is applied to the last three second-order time and spatial derivatives of Equation (1) at time step *n* and the $x = 1$ plane. Equation (1) can now be expressed as

$$\frac{U|^{n-1}_{1,j,k} - U|^{n-1}_{2,j,k}}{\Delta t \Delta x} - \frac{U|^n_{1,j,k} - U|^n_{2,j,k}}{\Delta t \Delta x} - \frac{U|^{n+1}_{1,j,k} - 2.U|^n_{1,j,k} + U|^{n-1}_{1,j,k}}{v\Delta t^2} + \frac{v\left(U|^n_{1,j+1,k} - 2.U|^n_{1,j,k} + U|^n_{1,j-1,k}\right)}{2.\Delta y^2} + \frac{v\left(U|^n_{1,j,k+1} - 2.U|^n_{1,j,k} + U|^n_{1,j,k-1}\right)}{2.\Delta z^2} = 0 \quad (10)$$

By moving the field components of time step *n* and $n-1$ to the right-hand side, Equation (10) is rewritten as Equation (11):

$$U|^{n+1}_{1,j,k} = 2U|^n_{1,j,k} - U|^{n-1}_{1,j,k} - \frac{v\Delta t}{\Delta x}\left(U|^n_{1,j,k} - U|^n_{2,j,k}\right) + \frac{v\Delta t}{\Delta x}\left(U|^{n-1}_{1,j,k} - U|^{n-1}_{2,j,k}\right) + \frac{1}{2}\left(\frac{v\Delta t}{\Delta y}\right)^2.\left(U|^n_{1,j+1,k} - 2.U|^n_{1,j,k} + U|^n_{1,j-1,k}\right) + \frac{1}{2}\left(\frac{v\Delta t}{\Delta z}\right)^2.\left(U|^n_{1,j,k+1} - 2.U|^n_{1,j,k} + U|^n_{1,j,k-1}\right) \quad (11)$$

As mentioned earlier, this ABC formulation exhibits a late-time instability that is improved over the early-time instability of the traditional Mur's ABC for magnetized plasma. Thus, to further delay the start of this late-time instability, we intentionally multiply the newly updated field components along the ABC boundaries each time step by a stability control factor s slightly less than 1.0. Then, Equation (11) above is reexpressed as Equation (12) below (wherein $s = 1.0$ yields the original ABC Equation (11)). It is expected that this multiplication factor will increase the level of reflection from the boundary, but it will further improve the stability (in the extreme case, $s = 0.0$ yields a PEC boundary wherein all the wave are fully reflected, but the algorithm is completely stable). Equation (113) is the final ABC expression for $x = 1$ boundary. It is used to terminate the magnetized cold plasma algorithm developed. Similarly, the ABC expressions for all other outer boundaries can also be derived in a same manner and the resulting formulations are shown as Equations (13) - (17).

$$x = 1 \rightarrow U|^{n+1}_{1,j,k} = \text{s.}\Big\{2.U|^n_{1,j,k} - U|^{n-1}_{1,j,k} - \frac{v\Delta t}{\Delta x}\left(U|^n_{1,j,k} - U|^n_{2,j,k}\right) + \frac{v\Delta t}{\Delta x}\left(U|^{n-1}_{1,j,k} - U|^{n-1}_{2,j,k}\right) + \frac{1}{2}\left(\frac{v\Delta t}{\Delta y}\right)^2.\left(U|^n_{1,j+1,k} - 2.U|^n_{1,j,k} + U|^n_{1,j-1,k}\right) + \frac{1}{2}\left(\frac{v\Delta t}{\Delta z}\right)^2.\left(U|^n_{1,j,k+1} - 2.U|^n_{1,j,k} + U|^n_{1,j,k-1}\right)\Big\} \quad (12)$$

$$x = \mathrm{h} \rightarrow U|_{h,j,k}^{n+1} = \mathrm{s}.\Big\{2.U|_{h,j,k}^{n} - U|_{h,j,k}^{n-1} - \frac{v\Delta t}{\Delta x}\left(U|_{h,j,k}^{n} - U|_{h-1,j,k}^{n}\right) + \frac{v\Delta t}{\Delta x}\left(U|_{h,j,k}^{n-1} - U|_{h-1,j,k}^{n-1}\right) + \frac{1}{2}\left(\frac{v\Delta t}{\Delta y}\right)^2.(U|_{h,j+1,k}^{n} - 2.U|_{h,j,kn} + U|_{h,j-1,kn}) + 12\,(v\Delta t\Delta z)2.(U|_{h,j,k+1n} - 2.U|_{h,j,kn} + U|_{h,j,k-1n})$$

(13)

$$y = 1 \rightarrow U|_{i,1,k}^{n+1} = \mathrm{s}.\Big\{2.U|_{i,1,k}^{n} - U|_{i,1,k}^{n-1} - \frac{v\Delta t}{\Delta y}\left(U|_{i,1,k}^{n} - U|_{i,2,k}^{n}\right) + \frac{v\Delta t}{\Delta y}\left(U|_{i,1,k}^{n-1} - U|_{i,2,k}^{n-1}\right) + \frac{1}{2}\left(\frac{v\Delta t}{\Delta x}\right)^2.(U|_{i+1,1,k}^{n} - 2.U|_{i,1,kn} + U|_{i-1,1,kn}) + 12\,(v\Delta t\Delta z)2.(U|_{i,1,k+1n} - 2.U|_{i,1,kn} + U|_{i,1,k-1n})$$

(14)

$$y = \mathrm{m} \rightarrow U|_{i,m,k}^{n+1} = \mathrm{s}.\Big\{2.U|_{i,m,k}^{n} - U|_{i,m,k}^{n-1} - \frac{v\Delta t}{\Delta y}\left(U|_{i,m,k}^{n} - U|_{i,m-1,k}^{n}\right) + \frac{v\Delta t}{\Delta y}\left(U|_{i,m,k}^{n-1} - U|_{i,m-1,k}^{n-1}\right) + \frac{1}{2}\left(\frac{v\Delta t}{\Delta x}\right)^2.(U|_{i+1,m,k}^{n} - 2.U|_{i,m,k}^{n} + U|_{i-1,m,kn}) + 12\,(v\Delta t\Delta z)2.(U|_{i,m,k+1n} - 2.U|_{i,m,kn} + U|_{i,m,k-1n})$$

(15)

$$z = 1 \rightarrow U|_{i,j,1}^{n+1} = \mathrm{s}.\Big\{2.U|_{i,j,1}^{n} - U|_{i,j,1}^{n-1} - \frac{v\Delta t}{\Delta z}\left(U|_{i,j,1}^{n} - U|_{i,j,2}^{n}\right) + \frac{v\Delta t}{\Delta z}\left(U|_{i,j,1}^{n-1} - U|_{i,j,2}^{n-1}\right) + \frac{1}{2}\left(\frac{v\Delta t}{\Delta x}\right)^2.(U|_{i+1,j,1}^{n} - 2.U|_{i,j,1n} + U|_{i-1,j,1n}) + 12\,(v\Delta t\Delta y)2.(U|_{1,j+1,1n} - 2.U|_{i,j,1n} + U|_{i,j-1,1n})$$

(16)

$$z = p \rightarrow U|_{i,j,p}^{n+1} = s.\Big\{2.U|_{i,j,p}^{n} - U|_{i,j,p}^{n-1} - \frac{v\Delta t}{\Delta z}\left(U|_{i,j,p}^{n} - U|_{i,j,p-1}^{n}\right) + \frac{v\Delta t}{\Delta z}\left(U|_{i,j,p}^{n-1} - U|_{i,j,p-1}^{n-1}\right) + \frac{1}{2}\left(\frac{v\Delta t}{\Delta x}\right)^2.(U|_{i+1,j,p}^{n} - 2.U|_{i,j,pn} + U|_{i-1,j,pn}) + 12\,(v\Delta t\Delta y)2.(U|_{1,j+1,pn} - 2.U|_{i,j,pn} + U|_{i,j-1,pn})$$

(17)

III. Numerical Experiments

1.1. Accuracy studies

The performance of our ABC scheme is first evaluated by testing the reflection error in a 100 × 100 × 100-cell FDTD grid having an *x*-directed electric dipole source at its center with a Gaussian modulated sinusoidal waveform as

$$E_x = exp\Big[-\left(\frac{t-t_0}{t_w}\right)^2\Big] . \mathrm{Sin}\,(2\pi f_c \mathrm{t})$$

(18)

where $t_w = 2.93\mu s$, $t_0 = 2.2t_w$ and $f_c = 4.0\ MHz$ is the center frequency of the source. The lattice space increments in each Cartesian direction of the FDTD grid are $\Delta x = \Delta y = \Delta z = 5m$, the time step Δt is 0.97 times the Courant limit and the stability control factor is $s = 1$. The plasma medium has an electron density Ne of $1.86 \times 108m^{-3}$, which corresponds to the ionosphere at an altitude of about 90 km. A static background magnetic field of 1.0×10^{-5} Tesla of various orientations is applied to the plasma to approximately mimic the magnetic field of the Earth. Without loss of generality, the E_x field component is probed at a point in the same *xy*-plane as the source and 3 cells from the outer *y*-boundary. The relative reflection error $Error|_{i.j.k}^{n}$ of the ABC at time-step *n* and grid location (*i, j, k*) is then calculated by the method detailed in [10] and defined as

$$Error|_{1,j,k}^{n} = \frac{\left|E|_{i,j,k}^{n} - E_{ref}\,|_{i,j,k}^{n}\right|}{\left|E_{ref\,.max}\,|_{i,j,k}^{n}\right|}$$

(19)

where $E|_{i.j.k}^{n}$ is the electric field value recorded at the probing point, and the reference solution $E_{ref}\,|_{i.j.k}^{n}$ is obtained from a sufficiently large benchmark grid having no reflected signals from grid boundaries at the probing point over the time-stepping span of interest. The maximum amplitude of the reference fields over all time steps at grid location (*i, j, k*) is denoted as $E_{ref\,.max}\,|_{i.j.k}^{n}$.

Figure 1(a)-(c) illustrate the numerical results of the relative errors for different applied magnetic field directions. For Figure 11(a), a *z*-directed magnetic field is applied to the plasma ($B_z = -1.0 \times 10^{-5}$ T and $B_x = B_y = 0$ T). For Figure 1(b), an *x*-directed magnetic field is applied to the plasma in the upper half of the grid ($z \geq z_{max}/2$, $B_x = 1.0 \times 10^{-5}$ and $B_y = B_z = 0$ T) and a *z*-directed magnetic field is applied to the plasma in the lower half of the grid ($z < z_{max}/2$, $B_z = -1.0 \times 10^{-5}$ and $B_x = B_y = 0$ T), where z_{max} is the maximum number of grid cells in the *z*-direction. For Figure 1(c), a magnetic field with 45 degree codip and Azimuth angles is applied to the plasma ($B_x = B_y = 0.5 \times 10^{-5}$ and $B_z = -0.707 \times 10^{-5}$). For all the cases depicted in Figure 1(a)-(c), the reflection errors are seen to be less than ~ 5%, clearly demonstrating the ABC's capability to provide the same approximate level of error regardless of the applied magnetic field direction.

To further evaluate the newly-derived ABC's performance compared to the original Mur's ABC, the same simulation parameters of Figure 1(c) are repeated with the original Mur's ABC. Figure 1(d) shows that the maximum reflection error for the case of the original Mur's ABC is also around 5%, as for the ABC of this chapter.

Next, the same numerical experiments have also been repeated without ABC (PEC in place of the ABC) to compare its performance with a PEC boundary. The result with a simulation condition as in the case of Figure 1(c) is shown in Figure 2. In this test, the ABC is simply removed and replaced by a PEC boundary and the recorded electric field variation at the probing point is then compared to those obtained from the grid with ABCs and from the large reference grid. One can see

that the PEC boundary is obviously introducing much larger reflection signals compared to the ABC and the large reference grid cases.

3.2. Evaluation of the ABC's performance in dense plasma

In Section 3.1, we performed accuracy studies of the ABC at a relatively low altitude (~ 90km) of the ionosphere (therefore a relatively low density plasma). To study the ABC's performance at higher altitudes (more dense plasma), the same simulation of Figure 1(a) is repeated for progressively larger electron densities N_e. We find through a series of tests that the maximum reflection error remains at the same level as for Figure 1(a) until the electron density N_e is increased to a level such that the center frequency f_c of the source becomes near to the critical cutoff frequencies of the plasma.

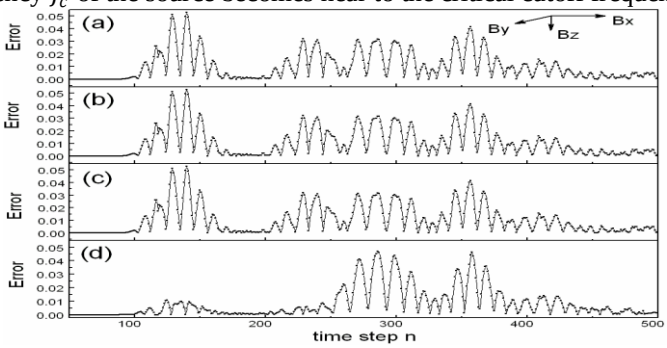

Figure.1. Reflection errors for different magnetic field directions applied to the plasma (a) B_x=B_y= 0 T, Bz= -1.0×10^{-5} T (b) B_x=1.0×10^{-5} and B_y=B_z= 0 T for z ≥ z_{max} /2, and B_z = $-1.0 \times 10^{-5}$and B_x= B_y= 0 T for z <z_{max} /2 (c) B_x=B_y= 0.5×10^{-5} and B_z= -0.707×10^{-5} (d) same magnetic field as in (c) applied to Mur's ABC.

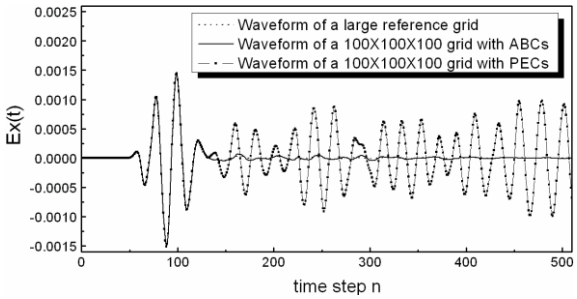

Figure.2. Time-domain electric field variations recorded at the probing point.

For example, Figure 3(c) illustrates the source spectrum employed in all of the numerical experiments. Figure 3(a) shows the dispersion diagram (wavenumber v.s. wave frequency) for the case of Figure 1(a) (a low-density plasma with N_e = 1.86×10^8 m^{-3} corresponding to an altitude of ~ 90km), and Figure 3(b) shows the dispersion diagram for a higher density plasma with N_e = 4.85×10^{10} m^{-3} (corresponding to an altitude of ~ 400km). The dotted lines of Figure 3(a) and Figure 3(b) represent the dispersion relation of the LHC-wave and the solid lines represent the dispersion diagram of the RHC-wave. We note that according to Figure.3, as N_e is increased from 1.86×10^8 m^{-3} to 4.85×10^{10} m^{-3} the source begins to have substantial spectrum below the cutoff frequencies of the LHC- and RHC-waves. This causes the portion of the source spectrum below ~ 2.1 MHz to change from propagating modes as for the case of Figure 3(a) to non-propagating modes as for the case of Figure 3(b). More importantly, though, closer to the cutoff frequencies, the phase velocity is increased. As a result, because a velocity of *c* corresponding to free space has been assumed for the ABC, the reflection error increases from ~ 5 % as for Figure.1(a) to ~ 6 % as shown in Figure.4(a) for the same scenario except for having an increasedN_e. To improve the accuracy, instead of using the free-space speed *c* for *v* in equations (1) - (6), the phase velocity *v* in the plasma at the source center frequency f_c is utilized, resulting in a value of ~ 1.13*c*. Figure 4(b) presents the results using *v* = 1.13 *c*, and as expected, the maximum reflection error is now reduced to ~ 4.5 % from ~ 6 % of Figure 4(a).

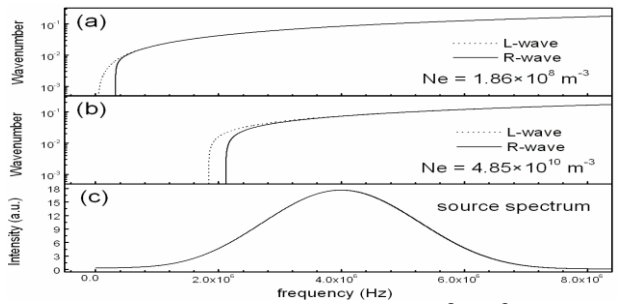

Figure.3. (a) dispersion diagram for a low-density plasma (N_e = 1.86×10^8 m^{-3}) (b) dispersion diagram for a high-density plasma (N_e = 4.85×10^{10} m^{-3}) (c) source wave spectrum

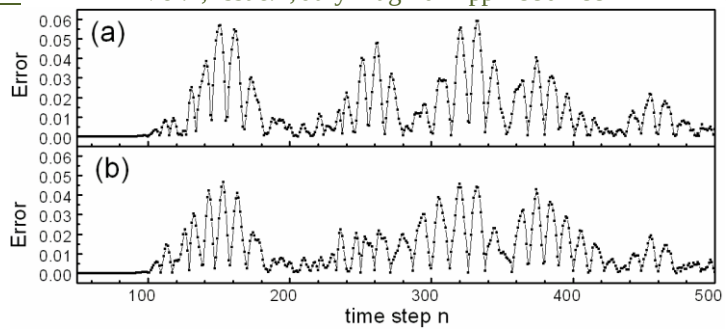

Figure.4. Reflection errors for a dense plasma (N_e = 4.85×10^{10} m^{-3}) (a) phase velocity *v* of the ABC assumed as free-space speed *c* (b) *v*=1.13*c*

IV. Conclusion

We find through longer numerical tests that the early-time instability of Mur's ABC is simply replaced by a late-time instability in Zhang and Wang's scheme. In this article, the feasibility of a variation of Zhang and Wang's scheme is investigated to serve as an effective ABC for the 3-D FDTD magnetized cold plasma formulation. We choose this scheme despite its inherent late-time instability because it has the potential to provide an acceptable level of error regardless of the direction of the background magnetic-field, a capability not provided by KPML. We then presented a simple but very effective way to 60 further delay the late-time instability of this magnetized plasma ABC. In Section 2, the formulation of the ABC scheme is first derived. Next, in Section 3, the newly-developed ABC scheme is rigorously tested by evaluating its reflection errors for different cases.

References :

[1] J. P. Berenger, "A perfectly matched layer for the absorption of electromagnetic waves," *J. Comp.Phys.*, vol.114, pp.185–200, 1994.

[2] S. G. Gedney, "An anisotropic perfectly matched layer-absorbing medium for the truncation of FDTD lattices," *IEEE Trans. Antennas Propagat.*, vol. 44, pp. 1630–1639, Dec. 1996.

[3] J. A. Roden and S. D. Gedney, "Convolutional PML (CPML): an efficient FDTD implementation of the CFS-PML for arbitrary media," *Microwave Opt. Technol. Lett.*, vol. 27, no. 5, pp. 334–339, 2000.

[4] S. A. Cummer, "A simple, nearly perfectly matched layer for general electromagnetic media," *IEEE Microwave Wireless Compon. Lett.*, vol. 13, pp. 128–130, Mar. 2003.

[5] M. W. Chevalier, T. W. Chevalier, and U. S. Inan, "A PML Utilizing k-Vector Information as Applied to the Whistler Mode in a Magnetized Plasma*," IEEE Trans. Antennas Propagat.*, vol.54, no.8, August 2006.

[6] E. Becache, S. Fauqueux, and P. Joly, "Stability of perfectly matched layers, group velocities, and anisotropic waves," *J. Computational Phys.*, vol. 188, pp. 399–433, 2003.

[7] S. A. Cummer, "Perfectly matched layer behavior in negative refractive index materials," *IEEE Antennas Wireless Propag. Lett.*, vol. 3, 2004.

[8] T. W. Chevalier, U. S. Inan and T. F. Bell, "Terminal Impedance and Antenna Current Distribution of a VLF Electric Dipole in the Inner Magnetosphere," *IEEE Trans. Antennas Propagat.*, vol. 56, pp. 2454–2468, Aug. 2008.

[9] G. Mur, "Absorbing boundary conditions for the finite-difference approximation of time-domain electromagnetic field equations," *IEEE Trans. Electromgn. Compat.*, vol. EMC-23, Nov. 1981.

[10] J.-N. Hwang and F.-C. Chen, "Stability Analysis of the Mur's Absorbing Boundary Condition in the alternating direction implicit finite-difference method," *IET Microw. Antennas Propag.*, vol. 1, no. 3, June 2007.

[11] Z. Yusheng and W. Wenbing, "The Studies of the Stability of FDTD with Mur's Absorbing Boundary Condition of Second Order in 3-D Scattering Problems," *IEEE Microwave and Guided Wave Letters*, vol. 6, no. 3, March 1996.

[12] B. Engquist and A. Majda, "Absorbing boundary conditions for the numerical simulation of waves," *Math. Comp.*, vol.31, pp.629-651, 1977.